Passive Method for Reducing Temperature Sensitivity of a Microelectromechanical Seismic Accelerometer for Marsquake Monitoring Below 1 Nano-*g*

Huafeng Liu,[1,2,*] W.T. Pike,[1,†] Constantinos Charalambous,[1] and Alexander E. Stott[1]

[1] *Optical and Semiconductor Devices Group, Department of Electrical and Electronic Engineering, Imperial College London, London SW7 2AZ, United Kingdom*

[2] *MOE Key Laboratory of Fundamental Physical Quantities Measurement, School of Physics, Huazhong University of Science and Technology, Wuhan 430074, People's Republic of China*

(Received 4 July 2019; revised manuscript received 3 October 2019; published 26 December 2019)

Silicon-based accelerometers suffer from high temperature sensitivity due to the thermoelastic effect of silicon. In order to alleviate this effect for high-precision acceleration measurement, several technologies have been reported, including both active and passive approaches. However, the existing methods either use extra circuits and devices with more complexity and power consumption or affect the mechanical and electrical characteristics of the accelerometer suspensions. In order to eliminate those side effects, this paper introduces a passive approach, which applies silicon-solder-bilayer thermal actuators at the base of the suspension to passively compensate the thermally induced displacement of the accelerometer's proof mass, to reduce the thermoelastic response of the silicon-based accelerometers. The proposed thermal actuator based on the shrink-fit technology can provide stable bonding with silicon structures and leads to good agreement of the theoretical model with both the simulation and experimental results. The thermal actuator is applied to a micromachined vertical seismic accelerometer, which has a peak sensitivity of 0.3×10^{-8} m s^{-2} $(\sqrt{\text{Hz}})^{-1}$ for picking up seismic signals on Mars, to reduce its temperature sensitivity. Both the preliminary test of the displacement thermal response by a commercial laser displacement transducer and the thermal-cycling-experiment results with the readout electricity show that this passive method can reduce the temperature sensitivity of the silicon-based vertical seismic accelerometer by at least 2 orders of magnitude. By applying this technology and the wind and thermal shield (WTS), the overall temperature-related noise is 0.26×10^{-8} m s^{-2} $(\sqrt{\text{Hz}})^{-1}$ at 0.1 Hz, which is comparable to the intrinsic noise floor of the seismic accelerometer, meeting the mission's requirement. The temperature-compensated seismic accelerometer package has been used as the payload of the Interior Exploration using the Seismic Investigations, Geodesy, and Heat Transport (InSight) lander, which landed successfully on Mars on November 26, 2018, with the seismic accelerometers operating since Martian day (sol) 4.

DOI: 10.1103/PhysRevApplied.12.064057

I. INTRODUCTION

Silicon has been used to fabricate high-precision microelectromechanical-system (MEMS) accelerometers for about 30 years [1–3], with the aiming of replacing quartz-based accelerometers [4,5] for high-performance applications with a low cost. However, the main challenge of silicon-based MEMS accelerometers lies in a much higher temperature sensitivity of the resonant frequencies than of the quartz counterparts, caused by the strong temperature dependence of the silicon's Young's modulus [6]. Either for the displacement-sensing pendulum accelerometers or the force-sensing resonant accelerometers, the basis of the sensing element is a spring-mass system. As the temperature varies, the suspension stiffness changes, so that the scale factor of a silicon-based open-loop accelerometer varies correspondingly. In addition, the bias of silicon accelerometers under gravity drifts with temperature due to spring softening or hardening.

There are a number of techniques to compensate for this effect, including both active and passive methods. The application of temperature postcompensation algorithms is one of the most commonly used compensation technologies [7]. However, this method relies on higher-order thermal models and external temperature sensors and hence suffers from thermal lags and temperature-induced hysteresis [8]. Other active approaches include packaging in temperature-stabilized micro-ovens [9] or electricity tuning [10], both of which require extra electronics,

*huafengliu@hust.edu.cn
†w.t.pike@imperial.ac.uk

 © 2019 American Physical Society

devices, and power. Passive approaches use composite materials in the springs, for example, substrate doping [11–13] and oxide-refilled trenches [14]. However, the introduction of additional materials affects the quality factor and the electrical characteristics of the suspension beams. Therefore, new structures with self-temperature compensation or robustness to the environment are potential alternatives.

An example of this temperature-induced stiffness variation effect relates to the use of flexure to support the proof mass (PM) of an accelerometer in the presence of the gravitational field. The vertical axis of an accelerometer will experience a temperature-dependent sag that is equal to the gravitational acceleration g divided by the square of the resonant angular frequency ω_0. For instance, a 10-Hz accelerometer will sag 2.5 mm under Earth's gravity and drift 1.5 μm over 10 °C due to the temperature coefficient of the Young's modulus of silicon, compromising accurate sensing of the PM position. Hence, addressing the drift issue is the basis of a high-performance silicon-accelerometer design. Compared with frequency-based resonators, the challenge of improving the determination of the PM displacement in accelerometers is not primarily to stabilize the resonant frequency but to compensate the variation of the thermally induced sag that can dominate the measurement. For instance, the MEMS gravimeter for Earth-tides measurement [15], which is a silicon flexure-based accelerometer with optical displacement sensing, has the sag displacement of the PM respond both to gravitational-field variations and temperature changes. The temperature sensitivity of the MEMS gravimeter is about 25×10^{-5} m s^{-2} °C^{-1}; therefore, it uses active temperature control to maintain the temperature of the system to within 0.001 °C to obtain an uncertainty of 25×10^{-8} m s^{-2}. However, for the subnano-g silicon seismic accelerometer with a peak sensitivity of 0.3×10^{-8} m s^{-2} $(\sqrt{\text{Hz}})^{-1}$ [16,17], the temperature-induced uncertainty is still too large, even using a similar high-precision temperature-control system.

Hence, in this paper, we perform a comprehensive study on the method of reducing the temperature sensitivity of the subnano-g MEMS seismic accelerometer for marsquake monitoring [18] . According to the previous temperature measurements on the surface of Mars [19], thermal effects are expected to be the major noise injection directly into the Mars seismic accelerometers. Therefore, thermal compensation is necessary. However, none of the existing methods can solve this thermal-drift issue without using ovens with extra circuits and sensors in terms of active compensation or affecting the mechanical and electrical characteristics of the suspension in terms of passive compensation. Hence, a passive approach, which uses thermal actuation to tilt the suspension support instead of affecting the suspension itself, has been developed.

II. PRINCIPLE OF THERMAL COMPENSATION

The basis of the proposed passive thermal-compensation approach is to use the thermally induced deflection of a bilayer structure at the base of the suspension to produce an angular strain. As the temperature is elevated, the PM of the accelerometer is driven upward by the angular strain to work against the suspension-softening-induced sag drift of the PM. The overall effect should be a minimum motion of the PM due to temperature variations.

The bilayer structure is inspired by a typical bimetallic strip shown in Fig. 1. Two types of metal with different coefficients of thermal expansion (CTEs) provide different expansions with temperature changes. If two metal layers are bonded or bolted together, the difference in their expansion will introduce an angular strain to bend the flat strip. With one end fixed and the other end free, this bimetallic strip gives an angle of θ that is temperature-dependent.

In order to illustrate the sag-shift issue, a cantilever-mass model is used, as shown in Fig. 2(a). The displacement of the PM can be derived according to Hooke's law:

$$x_0 = \frac{mg}{k}. \tag{1}$$

The spring constant k can be expressed as

$$k = \frac{3EI}{L^3}, \tag{2}$$

where E is the Young's modulus of the materials, $I = wt^3/12$ is the area moment of inertia of a thin beam, and L is the length of the cantilever. Hence, the sag displacement of the PM under gravity x_0 can be derived as

$$x_0 = \frac{4mgL^3}{Ewt^3}. \tag{3}$$

However, the Young's modulus and the dimensions of the beam are all temperature dependent. Hence, the overall sag

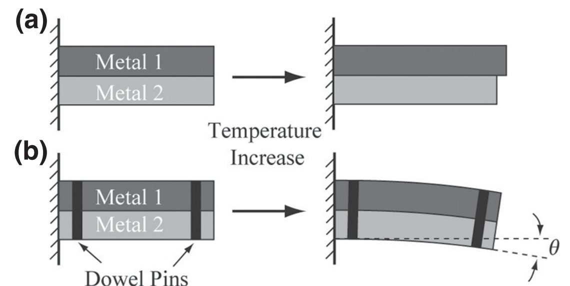

FIG. 1. (a) A bimetallic strip without bonding. (b) A bimetallic strip bolted by dowel pins.

displacement x also varies with temperature, having

$$x = x_0 + x(T) = \frac{mg}{k(T)} = \frac{4mgL^3(T)}{E(T)w(T)t^3(T)}. \tag{4}$$

Assuming that the material has an isotropic elasticity and a linear thermal coefficient, the temperature dependence of the total sag displacement is

$$\begin{aligned}\frac{\partial x}{\partial T} &= -x_0\left(\frac{1}{E}\frac{\partial E}{\partial T} + \frac{1}{L}\frac{\partial L}{\partial T}\right)\\ &= -x_0(\alpha_E + \alpha_L).\end{aligned} \tag{5}$$

According to the literature, composite materials can be used such that the thermal coefficients α_E and α_L are equal but of opposite polarity. Figure 2(b) shows that this thermally induced sag can be compensated by tilting the base of the cantilever, without requiring the suspension materials to be changed. In this case, the total sag should be

$$x = \frac{mg}{k(T)} - L(T)\theta(T), \tag{6}$$

giving

$$\begin{aligned}\frac{\partial x}{\partial T} &= -x_0(\alpha_E + \alpha_L) - L\left(\theta\alpha_L + \frac{\partial \theta}{\partial T}\right)\\ &\approx -x_0(\alpha_E + \alpha_L) - L\frac{\partial \theta}{\partial T},\end{aligned} \tag{7}$$

where the tilt θ is always quite a small angle, such that $L\theta \ll x_0$, therefore validating the approximation.

For a fully compensated cantilever-mass system, the overall sag displacement of the PM should be equal to x_0 and independent of temperature, having $\partial x/\partial T = 0$. In this case, the demand of the tilt angle against the temperature should be

$$\frac{\partial \theta}{\partial T} = -\frac{x_0}{L}(\alpha_E + \alpha_L). \tag{8}$$

This tilt demand can be met using a bilayer structure that is similar to a bimetallic strip. In this case, the compensation mechanism is achieved by using a structure with a temperature-dependent bending angle $\theta(T)$ to offset the temperature-dependent material parameters, including the Young's modulus $E(T)$ and the dimensions $L(T)$.

III. SILICON-SOLDER BILAYER THERMAL-ACTUATOR EXPERIMENTS

The basic bilayer structure is shown in Fig. 3(a). The lever, which is connected on the bimetallic strip, translates the angular strain $\theta(T)$ of the bimetallic strip into a translational displacement at its free end. To produce this bending angle $\theta(T)$ in silicon structures, solder, which has a larger CTE than silicon, is introduced into silicon cavities to form a silicon-solder bilayer structure, as shown in Fig. 3(b). The silicon cavities and the cantilever beam can be fabricated simultaneously using the through-wafer deep-reactive-ion-etching (DRIE) process [16]. Off-the-shelf solder balls can be loaded into those silicon cavities and then reflowed to form solder cylinders in silicon cavities [20]. After cooling down to room temperature, the bilayer structure has an initial displacement, since stress has been built into the geometry due to the CTE mismatching of different materials. As the temperature changes, the bilayer structure could passively actuate to move objects at the lever end.

Based on the above-mentioned principle, the proposed thermal-actuator structure design is illustrated in Fig. 4, including a simplified theoretical model, a more complicated finite element analysis (FEA) model, and the as-fabricated thermal-actuator chip. The theoretical model of the proposed thermal actuator shown in Fig. 4(a) can be considered as a silicon-solder-silicon trilayer strip. Thus,

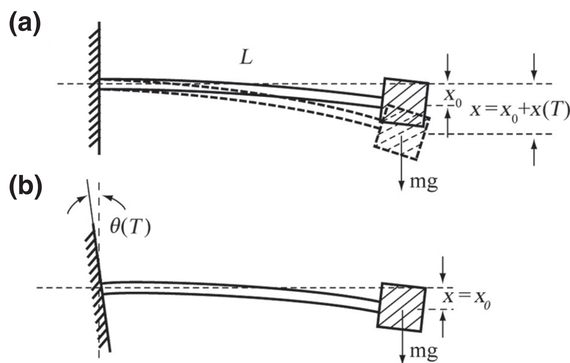

FIG. 2. (a) The PM suspended by a cantilever under gravity. (b) The PM lifted up by tilting the base of the cantilever.

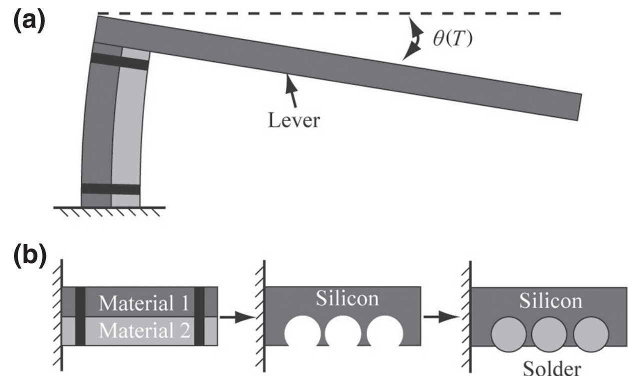

FIG. 3. The schematic design of the silicon-solder bilayer structure.

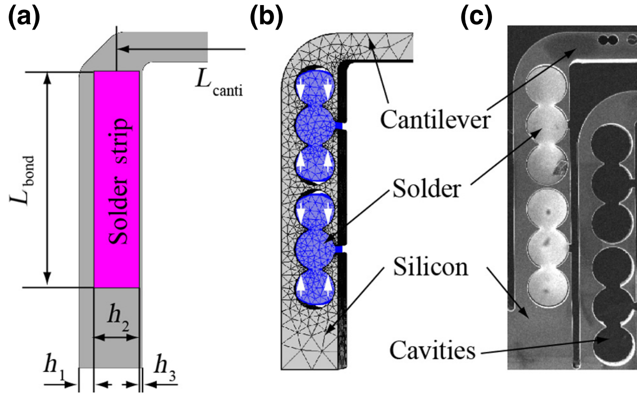

FIG. 4. The model and prototype of the silicon-solder thermal actuator: (a) the theoretical model; (b) the FEA model; and (c) the fabricated chip.

the closed-form solution of the temperature-dependent curvature can be derived as

$$\frac{1}{r} = f\ (E_i, h_i, \alpha_i)\ \Delta T, \tag{9}$$

where the function $f\ (E_i, h_i, \alpha_i)$ is given by the literature [21], E_i, h_i, and α_i are the Young's moduli, thicknesses and CTEs, respectively, of each layer and the subscripts 1, 2, and 3 represent the thicker silicon layer, the solder layer, and the thinner silicon layer, respectively. As the angular strain only occurs at the bonding area, the bending angle of the thermal actuator depends on the effective bonding length L_{bond}. Hence, the bending angle against temperature can be derived as

$$\frac{\Delta\theta}{\Delta T} = \frac{L_{bond}}{r}\frac{1}{\Delta T} = f\ (E_i, h_i, \alpha_i)\, L_{bond}. \tag{10}$$

Substituting Eq. (8) into Eq. (10) shows that to fully compensate for the temperature-dependent sag displacement $x(T)$, it is necessary that

$$f\ (E_i, h_i, \alpha_i)\, L_{bond} = -\frac{x_0}{L_{canti}}(\alpha_E + \alpha_L), \tag{11}$$

where L_{canti} is the cantilever length of the cantilever-mass model.

The challenge of implementing the thermal actuator lies in reliable bonding between the solder and the silicon; therefore, the shrink-fitting mechanism is introduced. In Fig. 4(b), the structure design of the proposed thermal actuator has two actuation units in series to be equivalent to the effective bonding length. For each unit, there is an optimized geometric silicon cavity with three holes in line. Solder balls can be loaded into the cavity and reflowed. Since solder has a larger CTE than silicon, when the temperature decreases solder is able to shrink faster than silicon and therefore the inner sides of the silicon cavities can be squeezed by the thermal stress, as the white arrows suggest. The strong shrink-fitting band is valid as long as the temperature is far lower than the melting point of the solder. In this case, the thermal deflection only relies on the geometry of the silicon cavities and the material properties of the solder, as the theoretical model suggests.

TABLE I. The parameters of the materials of each layer in the thermal actuator.

Parameters	Silicon	SAC305	Au80Sn20
Young's modulus E_i (GPa)	122	41	59.1
α_L (ppm °C^{-1})	2.6	23.5	16
Thickness h_i (μm)	72, 20	210	210
Reflow temperature (°C)	–	220	280

Several thermal-actuator chips are fabricated using the DRIE process. Solder balls with a diameter of 200 μm are used to fill the 525-μm-deep silicon cavities, with three balls for each hole. The chip with solidified solder is shown in Fig. 4(c). In order to verify the theoretical analysis, both FEA simulations and temperature-cycling experiments are conducted on the proof-of-principle chips. Both MEMS-compatible SAC305 [22] (3% silver, 0.5% copper, 96.5% tin) solder balls and Au80Sn20 (80% gold, 20% tin) [23] are used. The parameters of the multilayer structure, including the CTEs, the Young's moduli and the dimensions of both the solder and the silicon, are listed in Table I. Test chips are suspended at one side on the hot plate of a reflow rig, enabling the cantilevers to be friction free. The deflections of the thermal actuators against temperature are recorded by a digital camera through a translational microscope. The observed temperature-dependent deflections Δx over the cantilever length L_{canti} agree with both the theoretical and the FEA simulation results, as shown in Fig. 5. It can be seen that thermal actuators loaded with SAC305 solder had a larger temperature coefficient than Au80Sn20 solder, since SAC305 has both a larger CTE α_L and a larger Young's modulus E_i than Au80Sn20 solder. In this case, the principle of the silicon-solder thermal actuators is verified and the thermal response of the deflection has closed-form solutions.

IV. SEISMIC ACCELEROMETER THERMAL-COMPENSATION EXPERIMENTS

A. Structure of Mars seismic accelerometers

In this paper, the proposed silicon-solder thermal actuator is used to reduce the temperature sensitivity of the vertical seismic accelerometer for marsquake monitoring. The Mars seismic accelerometers, otherwise known as short-period (SP) seismometers, were designed to be one of the science payloads of the Interior Exploration using Seismic Investigations, Geodesy, and Heat Transport (InSight) Mars lander, which landed successfully on the surface of

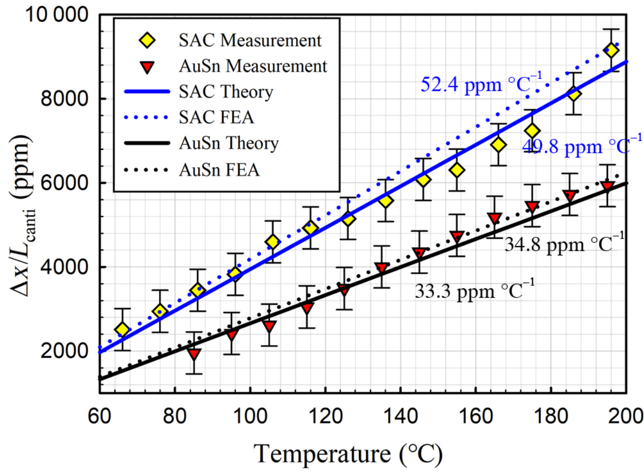

FIG. 5. The theoretical, FEA, and experimental results of the temperature coefficients of the thermal actuators with different solder (normalized).

Mars in November 2018 [24]. They are micromachined from single-crystal silicon using a through-wafer DRIE process to produce a suspension and a PM die with a fundamental frequency of 6 Hz in the in-plane vibrational mode. The suspensions of the horizontal accelerometer dies are symmetric, while for the vertical accelerometer the suspension is designed and fabricated in an offset geometry so that it will sag and take up a symmetrical configuration under Martian gravity. Figure 6 shows the vertical accelerometer die with the predefined offset geometry and thermal actuators.

On the surface of Mars, this vertical accelerometer would give an uncompensated thermal coefficient of $21 \times 10^{-5}\ \mathrm{m\,s^{-2}\,°C^{-1}}$ due to spring softening, which is considerably above the requirement of $5 \times 10^{-5}\ \mathrm{m\,s^{-2}\,°C^{-1}}$ [19]. To compensate for the thermal drift of the vertical accelerometer, the strength demands of the thermal actuators have to be worked out. Although spring-mass suspension systems vary according to the different designs, they can still be equivalent to a simple cantilever-mass

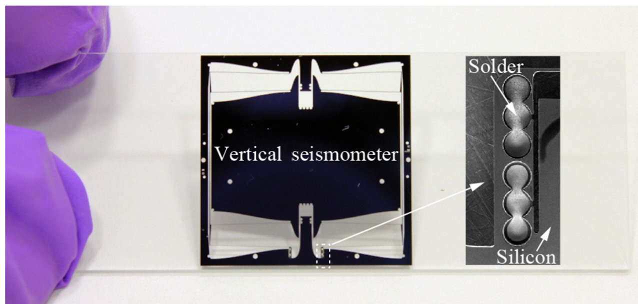

FIG. 6. A fabricated vertical MEMS seismic accelerometer (25 × 25 mm) with thermal actuators, tilted for demonstrating the operational status under Martian gravity.

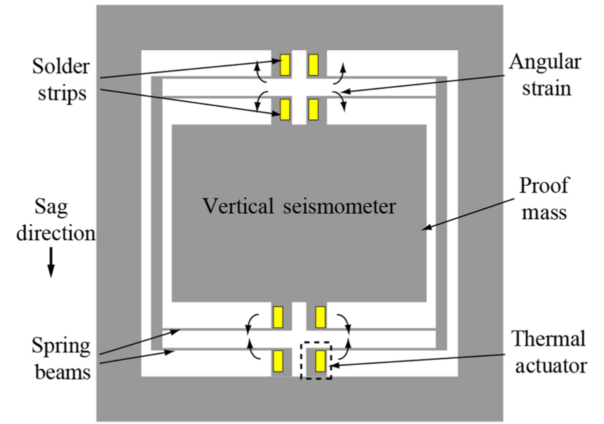

FIG. 7. An illustration of temperature compensation for the vertical seismic accelerometer with eight thermal actuators at the base of the silicon suspension; the arrows indicate the angular strain directions when the temperature increases.

system. For a given mass under gravity, an equivalent sag displacement of different suspension systems corresponds to the same stiffness:

$$k_{\mathrm{SP}} x_{\mathrm{sag}} = mg = k_{\mathrm{canti}} x_{\mathrm{sag}}. \tag{12}$$

As for the accelerometer design shown in Fig. 7, there are eight identical spring beams suspending the PM on the frame. The stiffness along the sag direction of the accelerometer, k_{SP}, is

$$k_{\mathrm{SP}} = \frac{24EI_{\mathrm{SP}}}{L_{\mathrm{SP}}^3}, \tag{13}$$

where L_{SP} and I_{SP} are the length and the area moment of inertia of the accelerometer spring beam, respectively.

Since the area moments of inertia of both the cantilever and the accelerometer suspensions have the same expression, the effective beam length of the accelerometer, which uses derived formulas from the cantilever-mass model, can be derived as

$$L_{\mathrm{canti}} = \frac{L_{\mathrm{SP}}}{2}. \tag{14}$$

Recalling Eq. (8), the required thermal actuation for the overall accelerometer suspension is derived as

$$\frac{\partial \theta}{\partial T} = -\frac{2x_0}{L_{\mathrm{SP}}}\left(\frac{\partial E/E}{\partial T} + \frac{\partial w/w}{\partial T}\right). \tag{15}$$

However, not all of the eight beams of the accelerometer can be equipped with the silicon-solder thermal actuators, since some supports of the accelerometer have electrical connection features on the surface. In this case, the available spring beams have to contribute more for the

overall compensation effect. In the practical SP seismic accelerometer design, only four beams in symmetric pairs are equipped with the thermal actuators. Thus, the required thermal actuation for each beam of the SP accelerometer can be derived as

$$\left.\frac{\partial\theta}{\partial T}\right|_{SP} = -\frac{x_0}{2L_{SP}}\left(\frac{\partial E/E}{\partial T} + \frac{\partial w/w}{\partial T}\right). \quad (16)$$

B. Preliminary test of thermal actuation

In order to preliminarily test the thermal-actuation effect on the seismic accelerometer, the thermal calibration experiment is conducted using the setup shown in Fig. 8. The accelerometer frame is suspended and fixed on the hot plate, which is tilted to a certain angle to match the reduced effect of Martian gravity (3.72 m s^{-2}). A LK-G5000 commercial laser displacement transducer [25] is aligned to position the laser spot on the side wall of the accelerometer PM and the diffusive reflection is sensed by a CMOS sensor inside the laser head. The high-precision laser head LK-H052 (Keyence) can provide a measurement repeatability of 25 nm [26]. As the temperature varies, the thermally induced motion of the PM is therefore determined.

The test chips are of the same design as the one shown in Fig. 6. They have a fundamental frequency of 6 Hz and a beam length of 9.3 mm. The thermal actuators have the same parameters as listed in Table I and are loaded with SAC305 solder balls. The results of displacements with varying temperature are plotted in Fig. 9 for both the test chips, with and without thermal actuation. The results show good agreement with both the closed-form and FEA-simulation results. The introduction of the thermal actuators reduces the temperature sensitivity of the seismic accelerometer from around −60 ppm °C^{-1} to less than 1 ppm °C^{-1}. Therefore, the thermal actuators are preliminarily validated to reduce the temperature sensitivity of the seismic accelerometers.

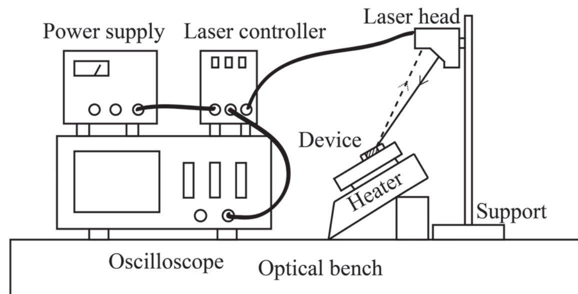

FIG. 8. The test setup to determine the thermal drift of a vertical seismic accelerometer under gravity.

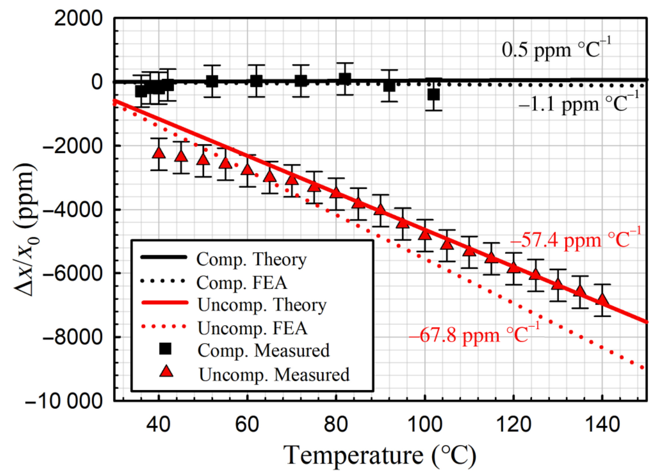

FIG. 9. A comparison of the displacement drift of the seismometer PM with and without thermal compensation.

C. Thermal response of Mars seismic accelerometers

The Mars-seismic-accelerometer package includes three single-axis seismic accelerometers consisting of two horizontal dies and one vertical die. For each accelerometer, the in-plane displacement of the PM is sensed by a capacitive displacement transducer (DT): two interposed arrays of electrodes on the PM are differentially driven and facing sets of fixed electrodes are plated on a fixed glass strip above the PM. The capacitance varies with the areal overlap of the driven and pickup electrodes, providing a displacement signal within the 96-μm periodicity of the array. The DT glass strip is connected both mechanically and electrically to the PM frame using solder thermocompression bonding, with pads at one end of the strip for electrical connection to the proximity electronics. The Mars seismic accelerometers operate in feedback mode with electromagnetic actuation from coils plated onto the PM die. Feedback is closed at the nearest null point of the periodic output of the DT die. This allows operation over a large tilt range while maintaining a low actuation force. The electrical connections to the coils and DT drives on the PM die are routed along the suspension flexures using sputtered and plated gold traces. As shown in Fig. 10, the sensor dies, magnets, and front-end electronics are hermetically sealed into an enclosure and the enclosure is evacuated and then back filled with nitrogen to 10 mBar to provide a stable internal environment. Feedthroughs on the base of the enclosure provide routing between the connector and the tether.

In order to clarify the thermoelastic model of the seismic accelerometer system, only the sensor die and the mounting structures are shown in Fig. 11. Each individual seismic accelerometer die is glued onto a Kovar-alloy frame through a compliant mounting and the frame is mounted onto the base of the enclosure via thermal-insulation

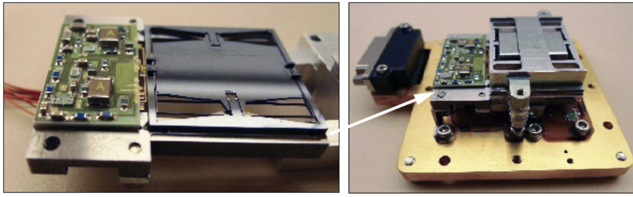

FIG. 10. A diagram of the seismic accelerometer assembly.

standoffs between the sensor and the enclosure. Thermal actuators are incorporated into the base of the vertical seismic accelerometer to attenuate the effect of temperature changes on the output. An approximately 1-kΩ resistor or resistance thermometer RT_{sensor} is sputtered onto the PM frame to allow direct monitoring of the sensor temperature. The other temperature sensor, RT_{enc}, a calibrated standard platinum-resistance thermometer, is mounted on the enclosure base, which is mechanically and thermally connected to the seismic laboratory leveling system of the InSight Mars lander.

Since thermal effects are expected to be the major noise injection of the seismic accelerometers on Mars [19], the temperature sensitivity of the seismic accelerometer needs to be minimized. There are three main thermal effects of the seismic accelerometer. The first effect is due to the temperature-dependent Young's modulus of silicon. For the horizontal seismic accelerometer dies, the Martian gravity vector is parallel to the symmetric suspension beams; therefore, the output bias will not be dominated by the spring softening or hardening. However, for the vertical seismic accelerometer die, this effect will cause movement of the PM under Martian gravity. The second thermal effect is for all the accelerometers and is due to CTE mismatching between the sensor and frame materials. The CTE-mismatching-induced thermal stress will cause tilts and therefore inject a component of gravity into the seismic accelerometer's outputs. In addition, the third thermal effect lies in the temperature-gradient-induced enclosure deformation and tilt. Here, the maximum temperature gradients are across the thermal insulation standoffs.

In this case, a simple lumped-element thermal model of the seismic accelerometers is constructed and the thermally

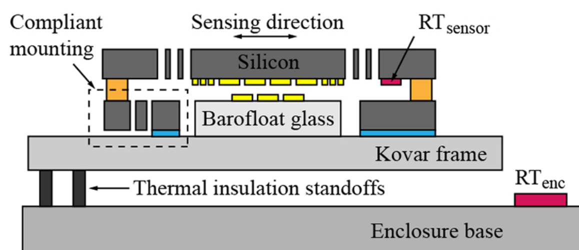

FIG. 11. A diagram showing the configuration of the Mars seismic accelerometers.

induced acceleration for each seismic accelerometer can then be expressed as

$$\Delta a_{\text{thermal}} = \alpha_{\text{sensor}} \Delta T_{\text{sensor}} + \alpha_{\text{enc}} \Delta (T_{\text{sensor}} - T_{\text{enc}}), \quad (17)$$

where α_{sensor} is the temperature sensitivity of the sensor due to spring softening or hardening and CTE-mismatching-induced tilt, α_{enc} is the temperature sensitivity of the enclosure deformation due to temperature gradients, ΔT_{sensor} is the temperature variation of the die, and $\Delta(T_{sensor} - T_{enc})$ is the variation of the temperature difference between the die and the enclosure.

Several technologies are applied to solve the thermal effect due to CTE mismatching. The CTEs of silicon, Barofloat 33 glass, and Kovar alloy are 2.6 ppm °C^{-1}, 3.25 ppm °C^{-1}, and 4.6 ppm °C^{-1}, respectively. According to the sensor configuration shown in Fig. 11, the CTE mismatching of the silicon-glass-based sensor die is matched to be within 0.5 ppm °C^{-1}. In addition, the compliant mounting structure, which is a much stiffer spring between the sensor and the mounting anchors, is applied to isolate the thermal stress from the Kovar frame. Therefore, the CTE-mismatching-induced thermoelastic response is minimized and α_{sensor} mainly depends on the spring-softening effect.

Although the spring-softening effect can be quantified by theoretical analysis, the overall resulting thermoelastic response is, however, difficult to predict. The temperature-gradient-induced thermoelastic response depends on non-nominal asymmetries in the thermal pathways, though it is expected to be proportional to the temperature difference between the sensor and enclosure temperatures. Therefore, an advanced alogrithm [27] is developed to extract the data for quantifying the thermoelastic response for the seismic accelerometer. The signal-processing method, which is based on decorrelation techniques, utilizes sensor fusion of seismic sensors and temperature sensors through an indirect Kalman filter to both characterize the seismic accelerometer and retrieve information from sensors in extreme environments.

In order to determine the model parameters and evaluate the thermal response of the seismic accelerometers, characterization experiments are conducted. One experiment is set up in the seismically quiet laboratory of the Atmospheric, Ocean, and Planetary Physics building at Oxford University. A vertical seismic accelerometer without thermal actuators, which is a qualification model (QM) sensor, is placed in a test chamber without temperature control and tilted to apply an acceleration equivalent to Martian gravity. The seismic accelerometer output is sampled at 100 Hz for 49 h by a 24-bit Centaur data logger [28]. The temperatures recorded by both the on-chip thermometer and the enclosure thermometer are between about 23.8 °C and 24.3 °C. A Guralp CMG-3T triaxial commercial seismometer [29] is placed alongside the test chamber

TABLE II. The thermal-sensitivity results of the vertical microseismometers with and without thermal compensation.

α_{sensor} Unit	Without compensation (10^{-5} m s^{-2} °C^{-1})	With compensation (10^{-5} m s^{-2} °C^{-1})
Theoretical	−21	0.19
FEA	−25	−0.41
Measured	−25 ± 1.2	−0.08 ± 0.28

to record the ambient seismic noise. The other experiment is performed in the French Centre National d'Etudes Spatiales (CNES) cleanroom in Toulouse. The vertical seismic accelerometer of the flight units, which has incorporated thermal actuators, is logged at 100 Hz over a controlled thermal cycling between 23 °C and 33 °C for 6.4 h by the 24-bit ADC of the Mars lander "Ebox." For both experiments, the outputs of the temperature sensors, RT_{sensor} and RT_{enc}, are recorded.

Those measured data sets are processed by applying the indirect Kalman-filter-based sensor-fusion technology. The completeness of the thermal model is assessed by repeating the multiple regression with a further node at an external temperature reference. In addition, both that theoretical analysis and the FEA simulations are conducted to estimate the temperature sensitivity of the sensor, α_{sensor}, due to spring softening or hardening. The measured results after processing agree well with the theoretical and FEA results for both the vertical QM die without thermal compensation and the vertical-flight-model (FM) die incorporated with the thermal compensators, as shown in Table II. The measured temperature sensitivity of the uncompensated vertical seismic accelerometer is -25×10^{-5} m s^{-2} °C^{-1}, while the temperature sensitivity of the compensated counterpart is -0.08×10^{-5} m s^{-2} °C^{-1}. Since the sensors with and without thermal compensation were of the same design, the results show that the thermal-compensation approach can reduce the temperature sensitivity of the sensor, α_{sensor}, by at least 2 orders of magnitude.

On the surface of Mars, the seismic accelerometer units are placed under WTS [30], which provides a stable environment with a temperature noise of 3×10^{-3} °C $(\sqrt{\text{Hz}})^{-1}$. According to the experimental data sets at Oxford, the data processing also works out the time constant of the thermal insulation standoff, at 467 s, a ratio of $\Delta(T_{sensor} - T_{enc})$ to ΔT_{sensor} of about 0.76×10^{-3}, and a temperature sensitivity of the enclosure α_{enc} of $-3.8 \pm 0.2 \times 10^{-4}$ m s^{-2} °C^{-1}. Therefore, recalling Eq. (17), for the slow temperature variation at 0.1 Hz, the vertical FM seismic accelerometer could have a thermally injected acceleration noise of 2.4×10^{-9} m s^{-2} $(\sqrt{\text{Hz}})^{-1}$ due to the sensor itself and 0.9×10^{-9} m s^{-2} $(\sqrt{\text{Hz}})^{-1}$ due to enclosure tilt. Since the decorrelation technology is used to separate the thermal effects of the sensors and the enclosure, the overall thermally injected noise density is equal to the square root of the summation of both the thermal-injection noise power due to the sensor itself and the enclosure tilt, which is 2.6×10^{-9} m s^{-2} $(\sqrt{\text{Hz}})^{-1}$ at 0.1 Hz and meets the mission requirements. The characterized FM-seismic-accelerometer units in this paper have been used as the payload of the InSight lander, which touched down on November 26, 2018, near Mars' equator, on the western side of a flat smooth expanse of lava plains called Elysium Planitia, with a signal affirming a completed landing sequence at 11:52 a.m. Pacific Standard Time [24]. According to the official announcement of the InSight Mission, the seismic accelerometers have been functioning well since sol 4 and have picked up the first signal that would seem to suggest a marsquake.

V. DISCUSSION

The horizontal seismic accelerometers do not apply the silicon-solder thermal-compensation technology, since the PM will not be subject to an appreciable component of gravitational acceleration. The CTE-mismatching-induced thermoelastic response of the horizontal accelerometers is also minimized by the compliant mounting structures. By using the same signal-processing technology, the thermal model parameters of one of the horizontal accelerometers is also determined, with a temperature sensitivity of the sensor die of $-3.72 \pm 0.15 \times 10^{-5}$ m s^{-2} °C^{-1} and a temperature sensitivity of the enclosure of $1.25 \pm 0.09 \times 10^{-4}$ m s^{-2} °C^{-1}. In the WTS environment, the horizontal seismic accelerometers also meet the mission's requirements.

The initial sag displacement x_0, which is essential for calculation of the thermal compensator strength in Eq. (8), is seen as constant and determined by the sag under gravity x_{sag}. However, the sag displacement is both time dependent and affected by the stress of shrink-fit bond-induced initial displacement x_{stress}, which can be expressed as

$$x_0(t) = x_{sag}(t) + x_{stress}(t). \tag{18}$$

The gravitational acceleration is time dependent due to the tidal effect and geological activity. Hence, the sag displacement $x_{sag}(t)$ of the seismic accelerometer at the same location is a function of time. In the silicon-solder structure, the creep effect of the solder will result in the loss of the prestress. Creep is a time-dependent deformation of a solid material, which happens under long-term and high-level stress below the yield strength [31]. Hence, the stress displacement $x_{stress}(t)$ is also a function of time. The creep studies of both SAC305 [32] and Au80Sn20 solder [33] suggest that the creep resistance drops with *both* the stress and an increase in temperature. However, the stress-induced displacement is at least 2 orders of magnitude smaller than $x_{sag}(t)$ and makes less of a contribution to the

overall sag displacement x_0. Hence, in terms of thermal compensation, the creep effect is negligible.

VI. CONCLUSION

This paper presents an approach that uses temperature-dependent silicon-solder structures to compensate for the thermal drift of low-frequency silicon suspensions subject to gravity by tilting the base of the suspension. Proof-of-principle thermal-actuator chips are designed and fabricated. Test results of their performance agree with both theoretical and FEA results. The proposed design is applied to a silicon suspension as a thermal compensator and the results demonstrate an attenuation of the thermoelastic response by 2 orders of magnitude compared to the uncompensated counterpart. This passive temperature-sensitivity-reduction approach is applied to the vertical seismic accelerometer for marsquake monitoring. The thermal-cycling experiment results show the temperature sensitivity of the vertical seismic accelerometer to be reduced from -25×10^{-5} m s^{-2} °C^{-1} to -0.08×10^{-5} m s^{-2} °C^{-1}. Within the wind and thermal shield, the thermally injected noise is 0.26×10^{-8} m s^{-2} $(\sqrt{\mathrm{Hz}})^{-1}$, meeting the requirements of the InSight Mars mission.

ACKNOWLEDGMENTS

We would like to thank Guangbin Dou and Anisha G. Mukherjee for preparing samples for the thermal actuators and fabricating the seismic accelerometer chips.

[1] F. Rudolf, A. Jornod, J. Bergqvist, and H. Leuthold, Precision accelerometers with μg resolution, Sens. Actuators A: Phys. **21**, 297 (1990).

[2] H. K. Rockstad, T. Kenny, J. Reynolds, W. Kaiser, and T. B. Gabrielson, A miniature high-sensitivity broad-band accelerometer based on electron tunneling transducers, Sens. Actuators A: Phys. **43**, 107 (1994).

[3] N. Yazdi, F. Ayazi, and K. Najafi, Micromachined inertial sensors, Proc. IEEE **86**, 1640 (1998).

[4] A. Kourepenis, A. Petrovich, and M. Weinberg, in *TRANSDUCERS'91: 1991 International Conference on Solid-State Sensors and Actuators. Digest of Technical Papers* (IEEE, San Francisco, California, USA, 1991), p. 551.

[5] S. A. Foote and D. B. Grindeland, Model QA3000 Q-flex accelerometer high performance test results, IEEE Aerosp. Electron. Syst. Mag. **7**, 59 (1992).

[6] M. A. Hopcroft, W. D. Nix, and T. W. Kenny, What is the Young's modulus of silicon? J. Microelectromech. Syst. **19**, 229 (2010).

[7] Y. Dong, P. Zwahlen, A. Nguyen, R. Frosio, and F. Rudolf, in *2011 16th International Solid-State Sensors, Actuators and Microsystems Conference* (IEEE, Beijing, China, 2011), p. 695.

[8] I. P. Prikhodko, A. A. Trusov, and A. M. Shkel, Compensation of drifts in high-*q* MEMS gyroscopes using temperature self-sensing, Sens. Actuators A: Phys. **201**, 517 (2013).

[9] J. C. Salvia, R. Melamud, S. A. Chandorkar, S. F. Lord, and T. W. Kenny, Real-time temperature compensation of MEMS oscillators using an integrated micro-oven and a phase-locked loop, J. Microelectromech. Syst. **19**, 192 (2010).

[10] H. Ko and D.-I. D. Cho, Highly programmable temperature compensated readout circuit for capacitive microaccelerometer, Sens. Actuators A: Phys. **158**, 72 (2010).

[11] A. Hajjam, A. Logan, and S. Pourkamali, Doping-induced temperature compensation of thermally actuated high-frequency silicon micromechanical resonators, J. Microelectromech. Syst. **21**, 681 (2012).

[12] A. K. Samarao and F. Ayazi, Temperature compensation of silicon resonators via degenerate doping, IEEE Trans. Electron. Devices **59**, 87 (2012).

[13] M. Shahmohammadi, B. P. Harrington, and R. Abdolvand, in *2012 IEEE International Frequency Control Symposium (FCS)* (IEEE, Baltimore, Maryland, USA, 2012), p. 1.

[14] M. Rais-Zadeh, V. A. Thakar, Z. Wu, and A. Peczalski, in *SPIE MOEMS-MEMS* (International Society for Optics and Photonics, San Francisco, California, USA, 2013), p. 86140E.

[15] R. Middlemiss, A. Samarelli, D. Paul, J. Hough, S. Rowan, and G. Hammond, Measurement of the Earth tides with a MEMS gravimeter, Nature **531**, 614 (2016).

[16] H. Liu and W. T. Pike, in *2015 Transducers-2015 18th International Conference on Solid-State Sensors, Actuators and Microsystems (TRANSDUCERS)* (IEEE, Anchorage, Alaska, USA, 2015), p. 916.

[17] W. T. Pike, S. Calcutt, I. Standley, A. Mukherjee, J. Temple, T. Warren, C. Charalambous, H. Liu, A. Stott, and J. McClean, in *Lunar and Planetary Science Conference* (The Woodlands, Texas, USA, 2016), Vol. 47, p. 2081.

[18] W. T. Pike, I. Standley, S. Calcutt, and A. Mukherjee, in *2018 IEEE Micro Electro Mechanical Systems (MEMS)* (IEEE, Belfast, Northern Ireland, UK, 2018), p. 113.

[19] D. Mimoun, N. Murdoch, P. Lognonné, K. Hurst, W. T. Pike, J. Hurley, T. Nébut, W. B. Banerdt, and SEIS Team, The noise model of the SEIS seismometer of the InSight mission to Mars, Space Sci. Rev. **211**, 383 (2017).

[20] A. Delahunty and W. T. Pike, Metal-armouring for shock protection of MEMS, Sens. Actuators A: Phys. **215**, 36 (2014).

[21] H. Torun and H. Urey, Thermal deflections in multilayer microstructures and athermalization, J. Appl. Phys. **100**, 023527 (2006).

[22] Senju-Metal-Industry, *Lead-Free Solder M705*, data sheet.

[23] Indium, *Eutectic Gold/Tin Solder*, data sheet.

[24] W. T. Pike, P. Lognonné, W. Banerdt, S. Calcutt, I. Standley, D. Giardini, C. Charalambous, A. Stott, J. McClean, T. Warren, *et al.*, in *Lunar and Planetary Science Conference* (The Woodlands, Texas, USA, 2019), Vol. 50.

[25] Keyence, *Ultra high-speed/high-accuracy laser displacement sensor: LK G5000 series* (), data sheet.

[26] Keyence, *Ultra high-speed/high-accuracy laser displacement sensor: LK H052* (), data sheet.

[27] A. E. Stott, C. Charalambous, T. J. Warren, and W. T. Pike, Full-band signal extraction from sensors in extreme environments: The NASA InSight microseismometer, IEEE Sens. J. **18**, 9382 (2018).

[28] Nanometrics, *Centaur Digital Recorder*, data sheet.

[29] Guralp, *Guralp CMG-3T Seismometer*, data sheet.

[30] P. Lognonné, W. Banerdt, D. Giardini, W. T. Pike, U. Christensen, P. Laudet, S. De Raucourt, P. Zweifel, S. Calcutt, M. Bierwirth, *et al.*, SEIS: Insight's seismic experiment for internal structure of Mars, Space Sci. Rev. **215**, 12 (2019).

[31] M. A. Meyers and K. K. Chawla, *Mechanical Behavior of Materials* (Cambridge University Press, Cambridge, 2009), Vol. 2.

[32] A. El-Daly, A. El-Taher, and T. Dalloul, Improved creep resistance and thermal behavior of Ni-doped Sn–3.0 Ag–0.5 Cu lead-free solder, J. Alloys Compd. **587**, 32 (2014).

[33] J. Elmer and R. Mulay, Superplastic creep of AuSn eutectic solder alloy, Scr. Mater. **120**, 14 (2016).